

MODELLING LOGIC GATES DESIGN USING PYRROLE BASED SINGLE MOLECULAR FIELD EFFECT TRANSISTOR

R. M. HARIHARAN, D. J. THIRUVADIGAL*

Centre for Materials Sciences and Nanodevices, Department of Physics and Nanotechnology, SRM University, Kattankulathur -603203, Tamil Nadu, India

In this work, we demonstrated the logic gate design using pyrrole based single molecular field effect transistor (FET) for the first time. The semi empirical quantum transport method, which is applying non-equilibrium Green's function (NEGF) in combination with self-consistent extended Huckel theory (SCEHT), has been adopted to study the charge transport characteristics of a modeled device. By using transmission characteristics $T(E)$, current-voltage I_{sd} - V_{sd} characteristics and molecular projected self-consistent Hamiltonian (MPSH) states, we systematically analysed charge transport characteristics of the pyrrole based single molecular FET. Theoretical results indicate that the external transverse gate bias can effectively tune the electronic transport properties of the molecular devices to a greater extent. The results exhibit that, with respect to the applied transverse gate bias V_g , the magnitude of the source-drain current I_{sd} varies over more than five times under the same source-drain bias V_{sd} . The gate controlled NDR feature, which is observed at the different V_{sd} bias, originates from the changes in the coupling degree between the molecular orbitals and electrodes. Finally, we demonstrate the application of using pyrrole based single molecular FET to realize five basic logic gates. The key feature of the suggested design is the opportunity of realizing different logic gates with just one molecular unit transistor.

(Received April 29, 2016; Accepted August 13, 2016)

Keywords: Molecular electronics, Single molecular FET, Gate field effect, Logic gate design

1. Introduction

One of the founders of Intel, Gordon Moore in 1970 foretold that the number of transistors crowded into integrated circuits would double every year, and "Moore's Law" was found correct in the past three decades [1-2]. This trend is being driven mainly by device miniaturization and therefore it is expected that in a few years we will reach a device size of a few nanometers. The endless demand for decrease in the size of the integrated digital electronic circuit has driven a quest for state-of-the-art devices at the nanometer scale [3-5]. This trend inspires the attention towards molecular electronics technology in which single molecules intrinsically nanometre in dimension are used as active electronic devices. Molecular electronics hold numerous benefits that make it to be a favourable technology. The molecular transistor is the key element of molecular electronics [6-9]. Field-effect transistors (FETs) made of individual molecules have proven to be the best substitute to silicon-based devices, due to their small size and superior performance.

Moreover, using such molecular FETs, various basic logic gates can be realized. In order to develop molecules into a remarkable substitute for Si-based devices, it would be essential to attain novel functionalities of the devices, or to implement the same functionality with very few transistors. Of late, the second approach is utilized to realize logic gates from a molecular field effect transistor of less count. Among several logic gates, XOR gate is the fundamental building blocks of digital encryption and parity checking electronics. Most of the fabricated logic gates, such as XOR gate, require at least four conventional FETs [10-11]. Very recently, Xu *et al.*,

* Corresponding author: john.d@ktr.srmuniv.ac.in

theoretically demonstrated five basic logic gate operations using gated single 1, 3- benzenedithiol molecular field effect transistor [12]. Benzenedithiol, a conjugated molecule has attracted a great deal of research attention in recent years due to their potential application in future generation electronic and optical devices.

Low band gap conjugated molecules are in the main focus in the ever growing field of condensed matter physics and organic electronics. Amongst the other wide range of conjugated systems other than benzenedithiol, heterocyclic molecules such as thiophene, furan and pyrrole takes a very special place owing to its unusual chemical stability and high conductivity [13-14]. But recent findings predict that pyrrole molecules have a high electron density when compared to their analogues with furan or thiophene. This higher electron density (in the pyrrole ring) can be explained by the different electric dipole moment of pyrrole compared to thiophene and furan, with its direction from the hetero atom to the five-membered ring, thus enhancing the contribution of the electrons of the nitrogen atom to the pi-system [15].

But so far pyrrole molecule based single molecular FET configuration was not reported largely. Therefore, to utilize pyrrole as backbone molecule is of great importance to the electronic transport properties of molecular devices of FET configuration and needs to be systematically investigated [16-17]. Here we demonstrate the realization of five basic logic gates with pyrrole based single molecular transistor. This was obtained by exploiting the transfer resistance of a single molecular transistor.

In this study, we demonstrate logic gate design using pyrrole based single molecular field effect transistor for the first time. The semi empirical quantum transport method, which is applying non-equilibrium Green's function (NEGF) in combination with self-consistent extended Huckel theory (SCEHT), has been adopted to study the effect of the transverse gate bias (V_g) on the conduction of pyrrole based single molecular FET and then to demonstrate the realization of five basic logic gates. The results show that the gate bias (V_g) has a crucial effect on the electronic transport properties of the molecular device. We found significant gate-tuned I_{sd} - V_{sd} characteristics. By using calculated source-drain resistance R as a function of V_g , we demonstrated designs of realizing five basic logic gates with gated molecular junction consisting single unit of pyrrole molecule.

2. Modeling and Theoretical Frame work

Geometry optimizations of pyrrole molecule with two S groups as linkers were carried out using Broyden-Fletcher-Goldfarb-Shanno (BFGS) method, which is a Quasi-Newton method. After that, optimized molecular structure is contacted to the gold electrodes through S-Au bonds after removing the H atoms from the S terminal groups. Au(111) electrodes with 3x3 atoms/layer was employed. In the optimized structure, estimated C-S (thiol end group) distance is 1.76 Å and measured S-Au distance is 2.39 Å. Then the pyrrole molecule was connected to contact electrodes (source and drain) through chemical bonding whereas the gate electrodes around it are electrically insulated from the molecule by dielectric materials. The whole system can be thought of as a hollow 3-D box with electrode plates as its sides inside which the molecule is placed. The sides of this box then define the boundary of the system. The dimension of the box is set by the molecular length, width, and the oxide thickness. Typically, for a two terminal system (i.e., when the gate electrodes are far away), the dimension of the box is set to be 100 Å x 100 Å x L where L is the molecular length. The molecule is placed 1.1 Å below a dielectric material with dielectric constant $\epsilon = 1.0$, corresponding to air medium. The dielectric is 2 Å thick and above the dielectric layer there is an electrostatic gate [18]. The schematic representation of gated single molecular device was shown in Fig. 1.

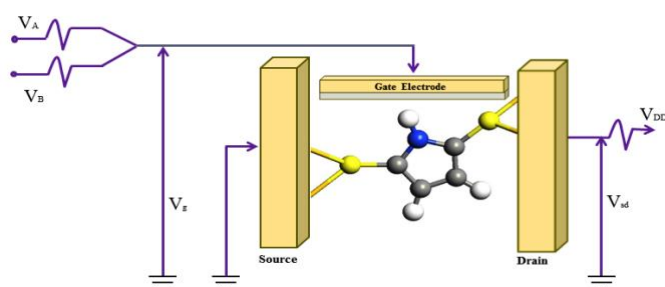


Fig. 1. Electrical circuit diagram of a two-inputs (A and B) logic gate incorporating single pyrrole molecular FET. The gate electrode has no effect on the source and drain electrodes. R is the output resistance of the junction, which depends on the gate voltage V_g .

The theoretical framework for the calculation of transport properties of the proposed system was presented in this section. The optimized pyrrole molecule inserted between two Au(111)-(3x3) left (source) and right (drain) electrodes through above mentioned anchoring group with a transverse gate electrode to form FET configuration. The geometrical optimization and the electronic transport properties calculations are carried out by a package Atomistix ToolKit (ATK, 11.2.3 version) [19], which is based on a combination of SCEHT method, along with a self-consistent description of the electrostatics and NEGF formalism. The non-equilibrium Green's function (NEGF) formalism accounts for quantum transport in molecular conductors out of equilibrium whereas self-consistent extended huckel theory (SCEHT) accounts for the electronic structures of the molecule and the contacts. This method has been used by several groups for a variety of applications and is well documented [20-22, 23].

In this theoretical framework, the Fermi level E_F of the electrodes was determined self-consistently by using the methodology introduced by Brandbyge *et al.*, [24]. Using this methodology, the charge transfer from the electrodes to the device region was included and all the electrostatic interactions were described self consistently. This was achieved by defining a real-space electron density and numerically solving for the Hartree potential on a real-space grid. Through a multigrid poisson solver, the self-consistent field from an applied bias and allow for including continuum dielectric regions and electrostatic gates within the scattering region [23].

The calculation of the electron-transport properties of the system was divided into two steps. The first step was a self-consistent calculation for the electrodes with periodic boundary conditions in the transport direction. In the directions perpendicular to the transport direction, we applied the boundary conditions for the two electrodes and the central region. In the second step of the calculation, the electrodes define the boundary conditions for a self-consistent open boundary calculation of the properties of the central region. The open boundary calculation was used to determine the density matrix. Then using density matrix, the real space density in the central region will be calculated. Once the real-space density is known, the Hartree potential is calculated by solving the Poisson equation [23],

$$-\nabla[\epsilon(\mathbf{r}) \nabla \delta V_H(\mathbf{r})] = \delta n(\mathbf{r}) \quad (1)$$

Here, $\epsilon(\mathbf{r})$ is the spatially dependent dielectric constant of the device constituents, allows for the inclusion of dielectric screening regions and $n(\mathbf{r})$ is the spatial distribution of the induced electron density. Poisson equation is solved with the appropriate boundary conditions on the leads and gate electrodes imposed by the applied voltages using a real-space multigrid method. The so-obtained Hartree potential defines a new Hamiltonian and the steps must be repeated until a self-consistent solution is obtained[23].

Once the self-consistent Hamiltonian has been obtained, we can finally evaluate the transmission coefficients [18, 23]

$$T(E) = \text{Tr} [\hat{\Gamma}_L(E) \hat{G}^\dagger(E) \hat{\Gamma}_R(E) \hat{G}(E)] \quad (2)$$

where $\hat{G}^\dagger(E)$ and $\hat{G}(E)$ are the retarded and advanced Green's functions of the scattering region and $\hat{\Gamma}_{L(R)}(E)$ are the broadening matrix, is defined by the lead self-energy term $\Sigma_{L(R)}$. And the source-drain current I_{sd} through the system is obtained by using Landauer-Buttiker formula

$$I = \frac{2e}{h} \int_{-\infty}^{\infty} T(E) [f(E - \mu_L) - f(E - \mu_R)] dE \quad (3)$$

where $\mu_{L(R)}$ are the chemical potentials of the left (right) electrode, $f(E - \mu_{L(R)})$ are the Fermi distribution functions of electrons in the left (right) electrode. Scattering region contains parts of the electrodes which includes the screening effects in the calculations. For the left and right electrodes, we used 3×3 unit cell in the x and y directions to avoid the interaction between the molecules and the mirror image. The Brillouin zone of the leads is sampled by $1 \times 1 \times 100$ k points in the directions of x, y and z (z is the electron transport direction), which is enough to produce the convergence. In the following sections, we apply this formalism to the calculation of the electrical properties of a pyrrole molecule in FET configuration.

3. Result and Discussions

3.1 Transmission Characteristics

To understand the mechanisms behind the changes in the electron transport properties of pyrrole based single molecular field effect transistor, we analysed transmission coefficient $T(E)$ at $V_{sd} = 0.0$ V for seven different values of V_g (-3.0, -2.0, -1.0, 0.0, 1.0, 2.0 and 3.0 V) (shown in Figure 2). The average Fermi level, which is the average value of the chemical potentials of the left and right electrodes, is set to zero. The first transmission peak that appears below and above the Fermi level E_F are assigned to the conduction properties through the highest occupied molecular orbitals (HOMO) and the lowest unoccupied molecular orbitals (LUMO) state of models respectively. From Figure 2, it was prominent that the resonance peaks are closer to Fermi level E_F in the HOMO region, therefore HOMO is the main transmission channel in this device. Also, we can see clearly the gate controlled modulation on Transmission Coefficients $T(E)$. A negative V_g will shift up the transmission peaks in the HOMO region relative to the E_F , whereas positive V_g will shift away HOMO transmission peaks from E_F as shown in Figure 2. For this reason, the magnitude of currents under positive V_g bias will be much lesser than under negative ones. The transmission coefficients $T(E)$ at Fermi level E_F ($V_{sd} = 0.0$ V) are 0.31, 0.24, 0.19, 0.13, 0.1, 0.08 and 0.065 for $V_g = -3.0, -2.0, -1.0, 0.0, 1.0, 2.0$ and 3.0 V, respectively. The transmission coefficient of $V_g = -3.0$ V at E_F is the highest, which results in the highest conductance for $V_g = -3.0$ V among all other $I_{sd} - V_{sd}$ curves in lower V_{sd} bias as shown in Figure 3.

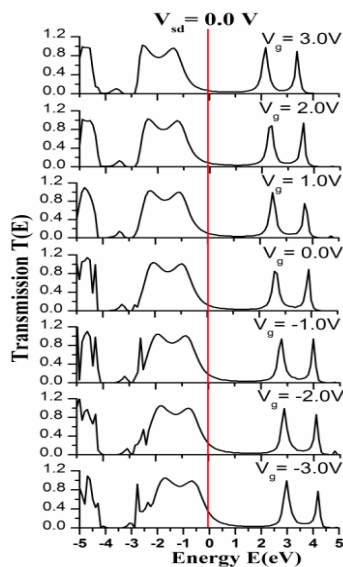


Fig. 2. Transmission spectra $T(E)$ at $V_{sd} = 0.0$ V for different gate bias $V_g = -3.0$ V, -2.0 V, -1.0 V, 0.0 V, 1.0 V, 2.0 V and 3.0 V, respectively. The red solid vertical line indicates the bias window.

3.2 I-V Characteristics

The self consistently calculated source-drain I_{sd} - V_{sd} characteristics are shown in Figure 3. The gate bias (V_g) is set to seven different values (-3.0 , -2.0 , -1.0 , 0.0 , 1.0 , 2.0 and 3.0 V) and V_{sd} was in a range from -4.0 to 4.0 V. The two most important features of the I_{sd} - V_{sd} curves were gate controlled current modulation and Negative Differential Resistance (NDR) feature. We can observe controllable gate-voltage dependence in this molecular junction.

It was observed that initially current through the molecular device increases with the increase in V_{sd} bias in the range of 0.0 to ± 2.5 V for both low positive bias and negative bias regime. The effect of the gate bias (V_g) on the I_{sd} - V_{sd} curves was clearly seen in this low bias regime. Significantly, for V_{sd} between 0 V and ± 2.5 V, the relation of current intensity I_{sd} were in relation as $V_g = -3.0$ V $>$ -2.0 V $>$ 1.0 V $>$ 0.0 V $>$ 1.0 V $>$ 2.0 V $>$ 3.0 V. It was clearly seen that the currents for $V_g = -3.0$ V show highest conductance, while that of $V_g = 3.0$ V shows least conductance in V_{sd} lower bias region as shown in the inset of Figure 3. It is found that magnitude of current varies more than five times for same V_{sd} over different V_g bias in both positive and negative bias regimes. For example, particularly for $V_{sd} = 1.4$ V, the I_{sd} is found to be 41.14 μ A at $V_g = -3.0$ V and 8.71 μ A at $V_g = 3.0$ V respectively. In this low bias regime, the electrons flow across the metal-molecule-metal junction via the non-resonant tunneling process under the influence of gate bias V_g and there by the molecules have ohmic behavior.

A deep attention at Fig. 3, reveals negative differential conductance behaviour in the transistor occurs above $V_{sd} = \pm 2.5$ V. Beyond voltage $V_{sd} = 2.5$ V, current through the molecular device diminishes with the increase in external bias voltage. The reduction in current due to the enhancement in external bias voltage is the manifestation of NDR. Figure 3, also reveals that above $V_{sd} = \pm 2.5$ V, gate bias V_g modulated NDR behaviour are observed at different V_{sd} between ± 2.6 V and ± 4.0 V. As V_g grows more negative, the magnitude of NDR effect increases and as V_g grows more positive, the magnitude of NDR effect decreases.

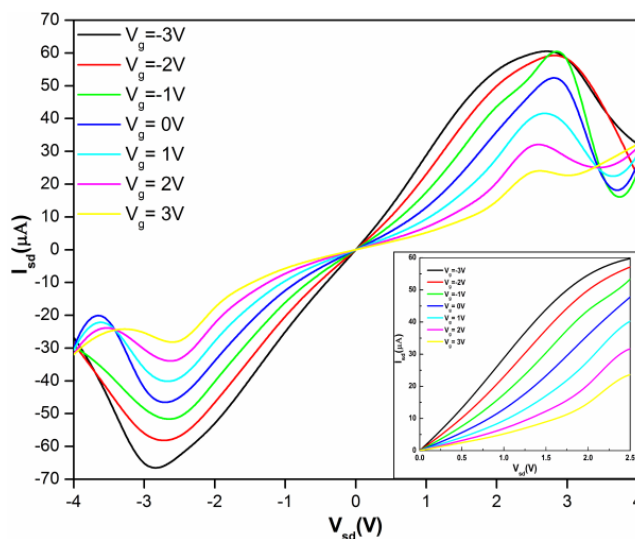


Fig. 3. Drain currents I_{sd} as a function of source – drain bias V_{sd} for different gate bias $V_g = -3.0V, -2.0V, -1.0V, 0.0V, 1.0V, 2.0V$ and $3.0V$. Inset: Drain currents I_{sd} as a function of V_{sd} for V_g in the bias range of 0 to +2V.

3.3 MSPH State analysis

According to the frontier molecular orbital theory, molecular electronic transport properties are determined to a great extent by the frontier molecular orbitals. From Transmission Spectra (see Figure 2), we find that molecular orbitals are modulated by the transverse gate bias applied to the molecule. This can be understood by relative positioning of highest occupied molecular orbital (HOMO) and lowest unoccupied molecular orbital (LUMO) with respect to Fermi level E_F for applied gate bias V_g . The HOMO positioned at $-0.66eV$ for $V_g = -3.0V$, $-0.92eV$ for $V_g = 0.0V$ and $-1.38eV$ for $V_g = 3.0V$, respectively. Similarly LUMO positioned at $2.98eV$ for $V_g = -3.0V$, $2.58eV$ for $V_g = 0.0V$ and $2.17eV$ for $V_g = 3.0V$, respectively. As V_g bias grows negative, the separation between LUMO and Fermi level E_F increases, whereas the separation between HOMO and Fermi level E_F decreases. Thus for the large negative bias the pyrrole act as n-type or an electron conduction molecule, while for the large positive bias, pyrrole act as p-type or hole conduction molecule. For $V_g = -3.0V$, the HOMO slightly falls on E_F , responsible for the molecular conduction for the entire range of V_{sd} bias.

To further understand the changes in the charge transport properties on applied gate voltages, we analyze molecular projected self-consistent Hamiltonian (MPSH) of four frontier molecular orbitals HOMO - 1, HOMO, LUMO and LUMO + 1 at $V_{sd} = 0.0V$ for different V_g , as shown in Figure 4. From Figure 4, we can observe that the both HOMO-1 and HOMO molecular orbitals were delocalised when V_g grow more negative. This results in high conductance. Although LUMO molecular orbitals are always delocalised (lesser than HOMOs) under negative V_g , they are far away from E_F and cannot be excited to transport electrons. Whereas on the contrary, under positive V_g , it can be observed that HOMO molecular orbitals are delocalised while HOMO+1, LUMO and LUMO+1 molecular orbitals remain localised, which results in low conductance.

3.4 NDR Feature

Another attractive phenomenon is the observation of NDR behaviour in the gated I_{sd} - V_{sd} curves. In order to understand it clearly, we show the transmission spectra obtained at different biases to explain the NDR behaviour in the positive bias V_{sd} of our device. In a recent work, Sen *et al.*, [25] explained the NDR behaviour by studying the shifting of transmission resonance peak across the bias window. To understand the NDR behaviour in our system, we observed the shifting of transmission resonance peak across the bias window at different bias voltages (V_{sd}) for different gate voltages (V_g).

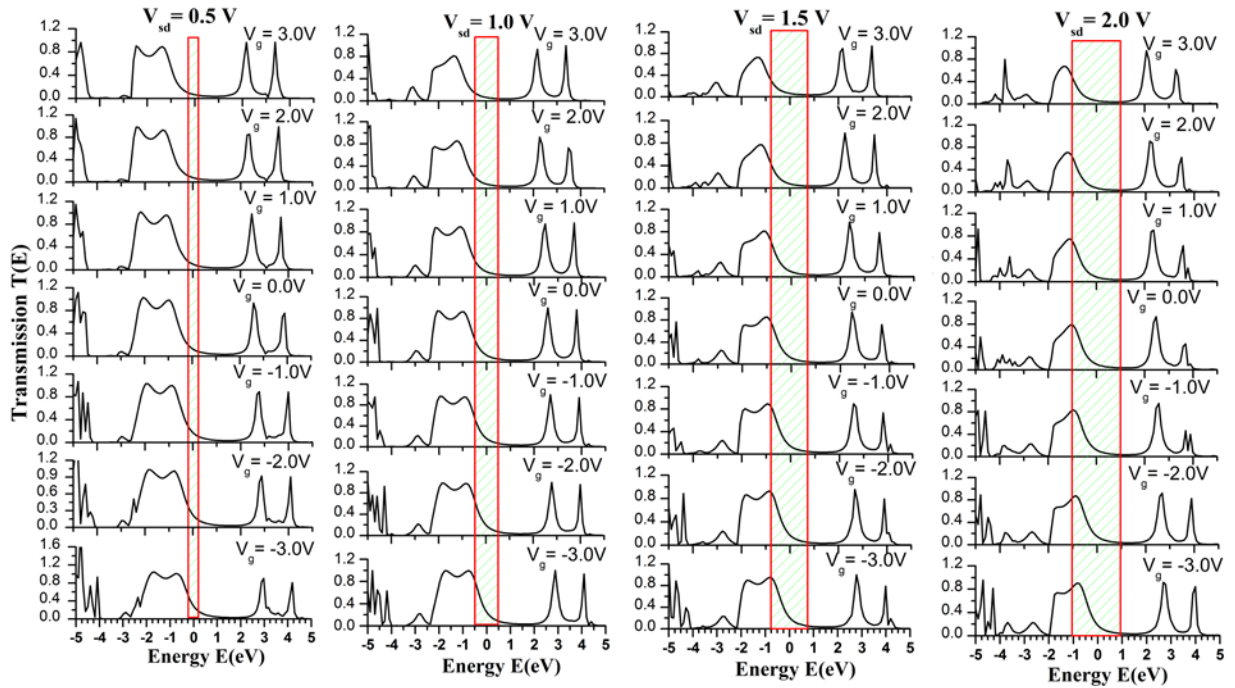


Fig. 5. Transmission Coefficient $T(E)$, at the positive bias V_{sd} of 0.5 V, 1.0 V, 1.5 V and 2.0 V, for different gate bias $V_g = -3.0V, -2.0V, -1.0V, 0.0V, 1.0V, 2.0V$ and 3.0V respectively. Shaded box region indicates the bias window.

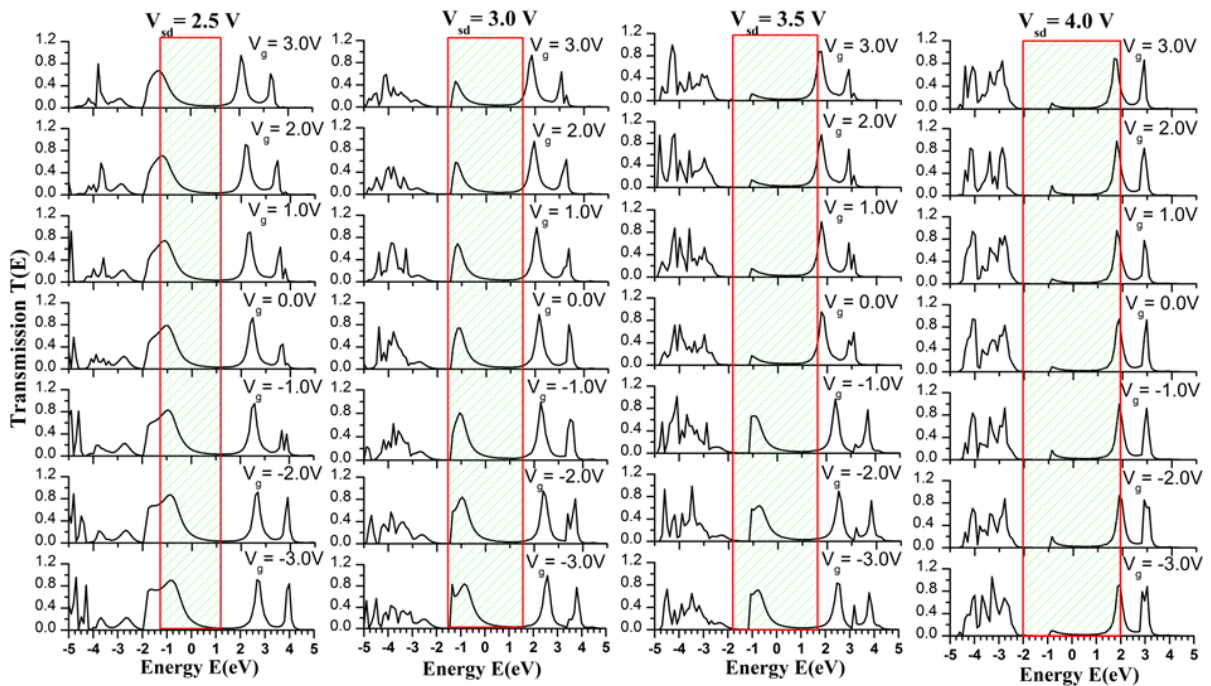


Fig. 6. Transmission Coefficient $T(E)$, at the positive bias V_{sd} of 2.5 V, 3.0 V, 3.5 V and 4.0 V, for different gate bias $V_g = -3.0V, -2.0V, -1.0V, 0.0V, 1.0V, 2.0V$ and 3.0V respectively. Shaded box region indicates the bias window.

The transmission spectra obtained at the positive bias voltages of 0.5, 1.0, 1.5, and 2.0V are presented in Figure 5. It is evident from Fig. 5 that, as V_{sd} increases, the bias window expands and the total integral area enlarges the contribution of the transmission resonance peak to the

bias window increases gradually. Consequently, the current through the FET system increases. A similar analysis of the transmission spectra corresponding to positive bias voltages of 2.5, 3.0, 3.5, and 4.0V reveal a gradual reduction of the transmission resonance peak within the bias window above 2.5V as shown in Fig. 6. As a result, current through the molecular systems diminish with the increase in positive bias voltage above 2.5 V and below 4.0V. Thus, within this bias window $V_{sd} = \pm 2.5$ to 4.0V bias range FET system would exhibit NDR character. From this we can infer that the transverse gate electrodes change the resonant transmission peaks and affect the coupling degree between the molecular orbitals and the electrodes, which resulted in NDR behaviours.

3.4 Logic Gate Scheme

Since the electronic transport properties of molecular devices can be effectively modulated by the external transverse gate electrodes, it makes a possibility of establishing FETs based on molecular devices. Here, we demonstrate an approach to realize five basic logic gates with only one single pyrrole molecular FET, at $V_{sd} = 3.83$ V, which is similar to the designing scheme proposed by Xu *et al.*, [12]. The electric circuit diagram is shown in the Figure 1. We present calculated source drain resistance as a function of V_g at $V_{sd} = 3.83$ V as shown in Fig. 7.

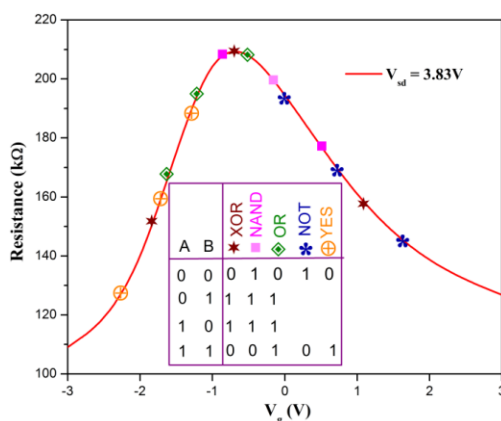


Fig. 7. Source-drain resistance (R) curve versus V_g at $V_{sd} = 3.83$ V. Every three equidistant operating points (marked by symbols) correspond to different functions of the logic gates.

We set V_g as an arithmetic mean of the two inputs V_A and V_B , namely, $V_g = (V_A + V_B)/2$. The two digital inputs V_A and V_B both have two values: low V_L (Boolean 0) and high V_H (Boolean 1) and therefore, V_g have three possible values: V_L (both inputs 0), V_H (both inputs 1) and $V_I = (V_L + V_H)/2$ (different inputs). If the voltage levels V_L and V_H are chosen such that the maximum of the curve is at $V_g = V_I$ and R has a smaller (and identical) value at $V_g = V_L$ or V_H (these three operating points are denoted by stars in Fig. 7), then an XOR gate is obtained. In this case, the resistance R is high (1) for different inputs and low (0) when both inputs are the same. Similarly, a NOT-AND (NAND) gate is obtained if the voltage levels are chosen such that the resistance R is high for $V_g = V_L$ or V_I and low for $V_g = V_H$. An OR gate is obtained if the resistance R is low for $V_g = V_L$ and high for $V_g = V_I$ or V_H . Finally, a NOT gate is obtained if the resistance R is high for $V_g = V_L$ and low for $V_g = V_H$. The complete truth table of the designed logic gates [26] is given in the inset of Figure 7.

To further understand the operation of each logic gate, we consider three equidistant operating points (marked by symbols) correspond to different functions of the logic gates as shown in Figure 7. An XOR gate (stars) is obtained for V_I (V_g of the middle point) = -0.7V and V_{GS} (total gate voltage swing) = 1.3V, a NAND gate (squares) for $V_I = -0.53$ V and $V_{GS} = 0.5$ V, an OR gate (diamonds) for $V_I = -0.81$ V and $V_{GS} = 1.42$ V, a NOT gate (clovers) for $V_I = 0.3$ V and $V_{GS} = 0.4$ V. Truth tables of all presented gates are shown in the inset of Figure 7.

The key feature of the suggested design is the opportunity of realizing different logic gates with just one molecular unit transistor. Despite such a low transistor count and small size, seems

very attractive, there are several other factors that should be considered in estimating a figure of merit. Although further improvements are required to approach the performance of conventional CMOS logic gates, the designed logic gates offer a promising alternative to conventional gates due to their minimal transistor count and small size.

4. Conclusion

Logic gate design is modeled using pyrrole based single molecular FET for the first time. The semi empirical quantum transport method, which is applying non-equilibrium Green's function (NEGF) in combination with self-consistent extended Huckel theory (SCEHT), has been adopted to study the effect of the transverse gate bias (V_g) on the charge transport properties of pyrrole based single molecular FET. The theoretical results specify that the I_{sd} currents can be effectively tuned by the gate electrode bias V_g . The results exhibit that, with respect to the applied transverse gate bias V_g , the magnitude of the source-drain current I_{sd} varies over more than five times under the same source-drain bias V_{sd} . This emphasizes the great importance of the transverse gate effect in single molecular transistors. The NDR feature, which is observed at the different V_{sd} bias, originates from the changes in the coupling degree between the molecular orbitals and electrodes. Finally, we demonstrate the application of using pyrrole based single molecular FET to realize five basic logic gates. The key feature of the suggested design is the opportunity of realizing different logic gates with just one molecular unit transistor.

Acknowledgement

The authors wish to thank Department of Science & Technology, Government of India. This work was supported by a grant from DST-FIST, Govt. of India (Grant Ref. No SR/FST/PSI-010/2010).

References

- [1] G. E. Moore, *Electronics* **8**, 114 (1965).
- [2] The International Technology Roadmap for Semiconductors 2013 Edition
- [3] A. Avarim, M.A. Ratner, *Chem. Phys. Lett.*, **29**, 277 (1974).
- [4] C. Joachim, J. K. Gimzewski and A. Aviram, *Nature*, **408**, 541 (2000).
- [5] J. Yao, Y. Li, Z. Zou, H. Wang, Y. Shen, *Superlattices and Microstructures*, **51**, 396 (2012).
- [6] H. Song, Y. Kim, Y.H. Jang, H. Jeong, M.A. Reed, T. Lee, *Nature*, **462**, 1039 (2009).
- [7] K. Xiao, Y. Liu, T. Qi, W. Zhang, F. Wang, J. Gao, W. Qiu, Y. Ma, G. Cui, S. Chen, X. Zhan, *J. Am. Chem. Soc.*, **127**, 13281 (2005).
- [8] B. Xu, X. Xiao, X. Yang, L. Zang, N. Tao, *J. Am. Chem. Soc.*, **127**, 2386(2005).
- [9] W. Jing, L. Yun-Ye, C. Hao, W. Peng, R. Note, H. Mizuseki, and Y. Kawazoe, *Chin. Phys. Lett.*, **27**, 067303 (2010).
- [10] S.M. Kang, Y. Leblebici, *CMOS Digital Integrated Circuits Analysis Design*, McGraw-Hill, New York, USA, (2002).
- [11] J. M. Wang, S. C. Fang, W.S. Feng, *IEEE J. Solid-State Circuits*, **29**, 780 (1994).
- [12] Y. Xu, C. Fang, B. Cui, G. Ji, Y. Zhai, D. Liu, *Appl. Phys. Lett.*, **99**, 043304 (2011).
- [13] W.W. Cheng, Y.X. Liao, H. Chen, R. Note, H. Mizuseki, Y. Kawazoe, *Phys. Lett. A*, **326**, 412, (2004).
- [14] C.P. Kala, P. ArunaPriya and D. John Thiruvadigal, *J. Comput. Theor. Nanosci.*, **10**, 213 (2012).
- [15] J. Pina, J.S.S. de Melo, R.M.F. Batista, S.P.G. Costa, M.M.M. Raposo, *Phys. Chem. Chem. Phys.*, **12**, 9719 (2010).
- [16] C. Xia, H. Liu, Q. Wang, *Adv. Mat. Res*, **152**, 931(2011).
- [17] K.Santanu, Y. Maiti and S. N. Karmakar, *Int. J. Mod. Phys. B*, **23**, 177 (2009).

- [18] F. Zahid, M. Paulsson, E. Polizzi, A.W. Ghosh, L. Siddiqui & S. Datta, *J. Chem. Phys.* **123**, 064707 (2005).
- [19] ATOMISTITIX TOOLKIT version 12.8.2, Quantum Wise A/S (www.quantumwise.com).
- [20] Ahmed Mahmoud, Paolo Lugli, *J. Appl. Phys.*, **116**, 204504 (2014).
- [21] C.P. Kala, P. ArunaPriya and D. John Thiruvadigal, *Commun. Theor. Phys.*, **59**, 649 (2013).
- [22] RM Hariharan and D. John Thiruvadigal, *Int. J. ChemTech Res.*, **7**, 706 (2014).
- [23] K. Stokbro, D.E. Petersen, S. Smidstrup, A. Blom, M. Ipsen, Kristen Kaasbjerg, *Physical Review B*, **82**, 075420 (2010).
- [24] M. Brandbyge, J.L. Mozos, P. Ordejón, J. Taylor, K. Stokbro, *Phys. Rev. B*, **65**, 165401 (2002).
- [25] S. Sen, S. Chakrabarti, *Comp. Mater. Sci.*, **45**, 889 (2009).
- [26] R. Sordan, F. Traversi, V. Russo, *Appl. Phys. Lett.*, **94**, 073305 (2009).